

Dissimilar permittivity and permeability sensitivities in nonlinear plasmons and spoof plasmons

Yen-Kai Chang^{1,2} and Chih-Wei Chang^{1,*}

¹Center for Condensed Matter Sciences, National Taiwan University, Taipei 10617, Taiwan

²Department of Physics, National Taiwan University, Taipei 10617, Taiwan

*Corresponding author: cwchang137@ntu.edu.tw

Received March 14, 2014; revised May 7, 2014; accepted May 14, 2014;
posted May 15, 2014 (Doc. ID 208191); published June 11, 2014

We show that employing localized surface plasmon resonators to probe environmental media will always lead to dissimilar optical sensitivities to permittivity and permeability. We find that while the permittivity sensitivities of diverse plasmonic structures display a geometry-independent universal scaling relation, the permeability sensitivities are highly dependent on the metals' geometries and resonant modes. Similar results are also found in mixed real/spoof localized surface plasmon resonators, and the phenomena can be universally scaled to the normalized effective plasmon frequencies. Importantly, the results put a fundamental constraint for all plasmonic-assisted nonlinear magneto-optical phenomena, including the Faraday effect, magneto-optical Kerr effect, and Cotton–Mouton effect. © 2014 Optical Society of America

OCIS codes: (250.5403) Plasmonics; (310.6628) Subwavelength structures, nanostructures.
<http://dx.doi.org/10.1364/OL.39.003607>

Many electromagnetic systems display identical responses to the environmental permittivity (ϵ) and permeability (μ). For example, the propagation constant (γ) of a rectangular waveguide of dimensions a and b as follows:

$$\gamma = i\sqrt{\omega^2\mu\epsilon - \left(\frac{m\pi}{a}\right)^2 - \left(\frac{n\pi}{b}\right)^2}, \quad (1)$$

where m and n are integers. Note that Eq. (1) yields identical results when exchanging ϵ and μ of the filled media. Physically, it means that one cannot distinguish whether the filled media is dielectric [$(\epsilon, \mu) = (x, 1)$] or magnetic [$(\epsilon, \mu) = (1, x)$] by measuring resonant frequencies, reflectance, or transmittance of the waveguide. The phenomenon is known to be applicable in many other electromagnetic systems, including microwave cavities and antennas.

Unlike microwave electromagnetic systems, plasmonic resonances arise from collective oscillations of electrons in metals; the presence of nonzero frequency at a long wavelength limit in bulk plasmons had been historically regarded as the first demonstration of acquiring mass via spontaneous symmetry breaking (i.e., Anderson–Higgs mechanism) [1]. Therefore, although plasmonic systems could yield a similar dispersion relation as a microwave waveguide, their origins should be fundamentally different. Because plasmonic resonant frequencies are sensitive to the environmental media, plasmonic nanostructures have been widely utilized for refractive index sensors. Recently, we have found that the refractive index sensitivities ($d\lambda_m/dn$, where λ_m is the resonant wavelengths of the m th harmonics, and n is the effective refractive index of the environment) for all kinds of individual or coupled plasmonic structures always linearly increase with λ_m/n and exhibit a slope equal to 1 [2]. Moreover, the universal scaling relation is found to be independent of the geometries or harmonic modes of the metal structures. However, due to the absence of magnetic resonances at optical frequencies, virtually all previous works have been limited to

investigating the plasmonic responses to dielectric media only. Besides, although the plasmon-assisted nonlinear magneto-optical effects have stimulated a lot of interest recently [3–5], it is not known about its fundamental limitations for enhancing the effects using surface plasmons.

In this Letter, we focus on studying the optical responses when employing localized surface plasmons as a probe for sensing dielectric and magnetic samples. We employ numerical simulations to compare the resonant wavelength redshifts ($\Delta\lambda_m$) of subwavelength plasmonic structures immersed in dielectric or magnetic media. As shown in Fig. 1, the resonant frequencies of a split-ring resonator (SRR) suspended in vacuum or immersed in dielectric [$(\epsilon, \mu) = (2, 1)$] or magnetic [$(\epsilon, \mu) = (1, 2)$] media are investigated using finite difference time domain simulation methods via commercial software (CST Microwave Studio). The resonant frequencies are identified from the dips of the simulated transmission spectra with fixed incident polarizations. To elucidate that dissimilar responses, the simulated materials to environmental ϵ and μ are fundamental properties of all plasmonic systems; the simulated materials are adjusted from PEC to Drude metals with arbitrary plasmon frequencies (we usually compare them with the plasmon frequency of gold, $\omega_{p, Au} = 2.175 \times 10^{15}$ Hz) and a damping rate of 1.2×10^{14} Hz. The sensitivity of the m th resonant mode of the SRR was obtained via $d\lambda_m/dn = \Delta\lambda_m/0.414$, as shown in Fig. 1.

The refractive index sensitivities of subwavelength structures (including SRRs, nanorods, and various kinds of nanoparticles) are generally described by either a standing wave model or Mie scattering theory. Recently, we find that the standing wave model is consistent with experimental and simulation results and yields a correct slope ($nd\lambda_m/(\lambda_m dn) = 1$) of the universal scaling relation rather than 2, as predicted by the Mie scattering theory [2,6].

According to the standing wave model, the resonant frequencies of a metal rod or an SRR can be characterized by the 1D standing wave model of surface plasmons [7]; i.e., $\lambda_m = 2n(L/m) - \lambda_0$, where λ_m is the resonant

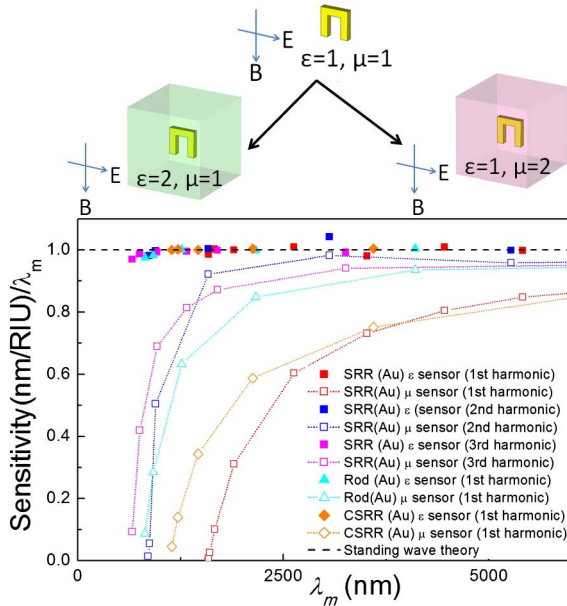


Fig. 1. (Top) Simulation procedures for determining the wavelength redshifts ($\Delta\lambda_m$) of an SRR when immersed into dielectric ($\epsilon = 1, \mu = 2$) or magnetic ($\epsilon = 1, \mu = 1$) media. Except for exchanging the media, all other simulated configurations, including the incident wave polarizations, remain unchanged. (Bottom) Normalized frequency-dependent ϵ sensitivity or μ sensitivity for various plasmonic metal structures and harmonic modes (SRR, split-ring resonator; Rod, nanorod; CSRR, split-ring resonator with complementary structures). Prediction of the standing wave model is plotted as a dashed line.

wavelength of the m th harmonic mode, L is the total length of the rod or the SRR, n is the effective refractive index of the environment, and λ_0 is a geometrically dependent offset. Because of $n = (\mu\epsilon)^{1/2}$, one might naively anticipate that the plasmonic responses to dielectric and magnetic media are identical, i.e., $d\lambda_m/d\epsilon^{1/2} = d\lambda_m/d\mu^{1/2}$.

Remarkably, our simulation results display otherwise. Figure 1 shows $d\lambda_m/d\epsilon^{1/2}$ and $d\lambda_m/d\mu^{1/2}$ as a function of λ_m for various metal structures, harmonic modes, and plasmon frequencies. It can be seen from Fig. 1 that, while the sensitivities to ϵ yields a universal scaling line (which is independent of structural geometries, harmonic modes, or plasmon frequencies), the sensitivities to μ deviate from the universal scaling line, and they gradually decrease to zero with decreasing λ_m . Particularly, one can always find a critical size for a metal structure beyond which the permeability sensitivity is nearly zero. Unlike microwave electromagnetic systems, the observed disparity between ϵ and μ sensitivities is inherent whenever employing plasmonic systems as probes for detecting environmental media.

We now quantify the result in terms of the ratio of ϵ sensitivities to μ sensitivities. As shown in Fig. 2(a), we find that, although the effect of plasmon frequencies to μ sensitivities can be rescaled to the respective plasmon frequencies, the deviation to the universal line is highly mode-dependent. For an SRR, the ratio of ϵ sensitivity to μ sensitivity at the first-harmonic resonance deviates from unity at a much lower frequency than do the second or third harmonic resonances. Similar

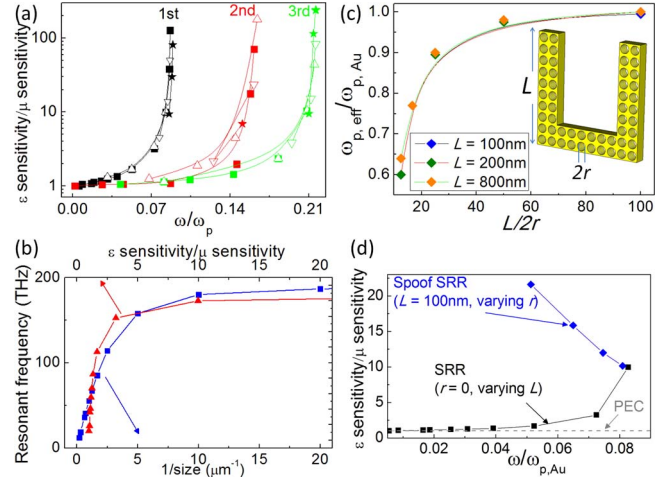


Fig. 2. (a) The ratio of ϵ sensitivity to μ sensitivity as a function of plasmon frequencies [1 (rectangle), 1/2 (up triangle), 1/5 (down triangle), and 1/10 (star) of $\omega_{p,\text{Au}}$], harmonic modes, and resonant frequency (normalized to the respective plasmon frequencies). (b) The saturation of resonant frequencies with reducing sizes of an SRR is similar to the curve of the ratios of ϵ sensitivity to μ sensitivity. (c) Normalized effective plasmon frequency ($\omega_{p,\text{eff}}/\omega_{p,\text{Au}}$) for different spoof SRRs shown in the inset. (d) The ratio of ϵ sensitivity to μ sensitivity as a function of resonant frequencies (normalized to $\omega_{p,\text{Au}}$) for SRRs and spoof SRRs. Here the resonant frequencies of SRRs and spoof SRRs are tuned by varying L and r , respectively.

behaviors are also observed in nanorods or complementary metal structures.

One may surmise the effect originating from the dispersion relation imposed in the simulation. The dispersion relation of Drude metals is known to lead to the saturation of resonant frequencies of SRRs at reduced sizes [8]. Similarly, when plotting the saturation of resonant frequencies together with the ratio of ϵ sensitivity to μ sensitivity [Fig. 2(b)], we find a resemblance between the two curves. The results suggest the origin of the effect arises from the dispersion relation of metals.

The saturation of resonant frequencies is known to be due to the added inductance of kinetic electrons of metals in an LC resonator, whose resonant frequency is characterized by the lumped inductor and capacitor [8]. Correspondingly, the ratio of ϵ sensitivity to μ sensitivity can be obtained:

$$\frac{\epsilon \text{ sensitivity}}{\mu \text{ sensitivity}} = \sqrt{\frac{\mu(L + L_e)}{\epsilon L}}, \quad (2)$$

where L is the geometrically determined inductance. L_e is the inductance of kinetic electrons of metals, and its contribution is independent of geometries or environmental media. From Eq. (2), one can anticipate dissimilar responses between $d\lambda_m/d\epsilon^{1/2}$ and $d\lambda_m/d\mu^{1/2}$ for any plasmonic structures. We have calculated and found it reproduces the results shown in Fig. 2(b), further justifying the LC resonator model for explaining the dissimilar sensitivities.

To investigate the validity of the LC resonator model, we now extend our studies to spoof plasmons, in which the dispersion relation is created by artificial geometrical

modifications of the metal structures. In spoof plasmons, grooves or holes with feature sizes much smaller than the wavelengths of incident waves are artificially made onto the surface of metal structures, thereby allowing electromagnetic fields to penetrate into the metal surface. Thus they can effectively create a dispersion relation similar to that of a Drude metal and support surface waves even in a PEC. Spoof plasmons were first studied in extended interfaces and recently applied to localized surface plasmons [9,10]. Naively, since the dissimilar sensitivities shown in Figs. 1 and 2(a) are due to the dispersion relation of metals, one might expect that spoof plasmons would mimic every aspect of real plasmons and yield dissimilar sensitivities as well. In the following, we will show that spoof plasmons alone do not lead to dissimilar sensitivities but they play an interesting role when mixed with real plasmons of metals.

The inset of Fig. 2(c) shows a representative structure of localized spoof plasmons, created by making many small holes (with radius r) in an SRR. These holes allow electromagnetic waves to further penetrate into the metal surface and thereby support surface waves. They also lead to redshifts of resonant frequencies compared with those of the pristine SRRs. Thus these subwavelength structures function as an effective plasmon frequency $\omega_{p,\text{eff}}$. The $\omega_{p,\text{eff}}$ can be obtained by simulating the transmission spectrum of a pristine SRR (i.e., without the holes) with adjustable $\omega_{p,\text{eff}}$ until it yields identical results as those of a spoof SRR. In Fig. 2(c), we show that $\omega_{p,\text{eff}}$ and r can be rescaled to a universal curve when they are normalized to the plasmon frequency of the metal and the length (L) of the SRR, respectively. Thus varying $L/2r$ of the spoof SRR can effectively reduce $\omega_{p,\text{eff}}/\omega_{p,\text{Au}}$ and change the dispersion relation.

Interestingly, although it is generally believed that spoof plasmons in a PEC can exhibit a dispersion relation with an $\omega_{p,\text{eff}}$, their ϵ and μ sensitivities remain identical. As shown in the horizontal dashed line of Fig. 2(d), both ϵ and μ sensitivities follow an identical universal line for various spoof SRRs made of PEC. In contrast, Fig. 2(d) shows dissimilar ϵ and μ sensitivities for SRRs with “real” plasmons, whose dispersion relation and plasmon frequency are intrinsic properties of the metal. Apparently, the metal-like dispersion relation is not a sufficient condition for yielding dissimilar sensitivities to environmental ϵ and μ . At first sight, the result seems to suggest that one can, in principle, distinguish whether a plasmon is “real” or “spoof” by testing the optical responses to environmental ϵ and μ . Furthermore, from the LC resonator model, one might also anticipate that introducing the subwavelength structures is simply a geometrical modification, and it would affect the L in Eq. (2) only. That is, one expects to see the ratio of ϵ sensitivity to μ sensitivity decrease with increasing L (or equivalently, decreasing resonant frequencies), similar to those observed in “real” localized plasmons.

Remarkably, when creating spoof plasmons in a Drude metal, the ϵ and μ sensitivities display distinct behaviors from those of real plasmons. As shown in Fig. 2(d), we find that the ratios of ϵ sensitivity to μ sensitivity increase with reducing resonant frequencies for spoof SRRs, whereas those of real SRRs show opposite trends. The

unexpected results indicate that the LC resonator model fails to explain the behavior of spoof SRRs.

Our further investigations show that the ratio of ϵ sensitivity to μ sensitivity obeys a universal curve once the resonant frequencies are normalized to their respective $\omega_{p,\text{eff}}$. Here the effective plasmon frequency $\omega_{p,\text{eff}}$ can either originate from the “real” plasmon frequencies of Drude metals (i.e., $\omega_{p,\text{eff}} = \omega_{p,\text{Au}}$) or from mixed effects of spoof plasmons and real plasmons [whose $\omega_{p,\text{eff}}$ is determined from Fig. 2(c)]. As shown in Fig. 3, the effects of “real” or spoof plasmons cannot be distinguished from each other once they are mixed. Therefore, although the spoof plasmons in a PEC always yields identical ϵ and μ sensitivities, once they are mixed with real plasmons of metals, their effects cannot be distinguished from those of real plasmons exhibiting $\omega_{p,\text{eff}}$.

Away from the (effective) plasmon frequencies, the difference between ϵ and μ sensitivities decreases rapidly. For example, we estimate the ratio of ϵ sensitivities to μ sensitivities deviates from unity by $\sim 10^{-6}$ at 100 GHz for copper. On the other hand, although the absence of magnetic resonances at optical frequencies indicates difficulties in observing the effect within the linear optics domain, the effect can be important in nonlinear optics.

Employing localized surface plasmons to enhance/probe nonlinear optical phenomena has two kinds of effects. First, localized surface plasmonic resonances can lead to electromagnetic hot spots and enhance the nonlinear effects. Second, the induced nonlinear refractive index changes can be probed by the localized plasmonic structures. Recent theoretical and experimental progresses on enhancing the magneto-optical Kerr effect or the Faraday effect via surface plasmons are based on the two effects [3–5]. In the following, we will show how the results discussed in the previous sections put fundamental constraints on both effects.

In general, the energy (U) of a nonlinear media can be expressed as

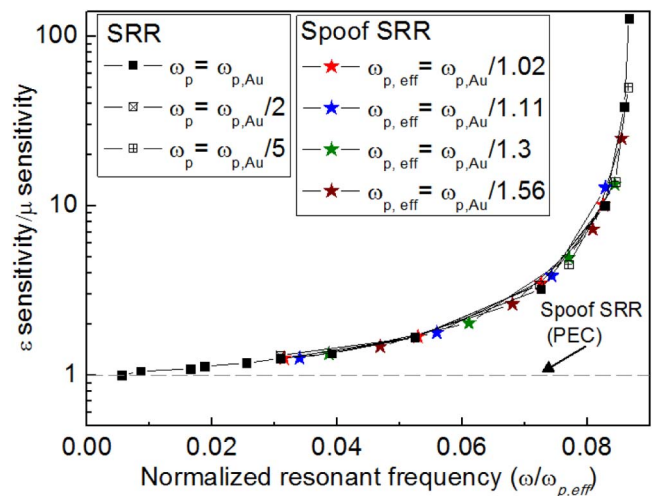


Fig. 3. Universal relation for the ratio of ϵ sensitivity to μ sensitivity as a function of resonant frequencies. The resonant frequency is normalized to the plasmon frequency (1, 1/2, and 1/5 of $\omega_{p,\text{Au}}$, respectively) for SRRs and to $\omega_{p,\text{eff}}$ [determined from Fig. 2(c)] for spoof SRRs, respectively. When the spoof SRR is made by PEC, identical ϵ and μ sensitivities are observed (dashed line).

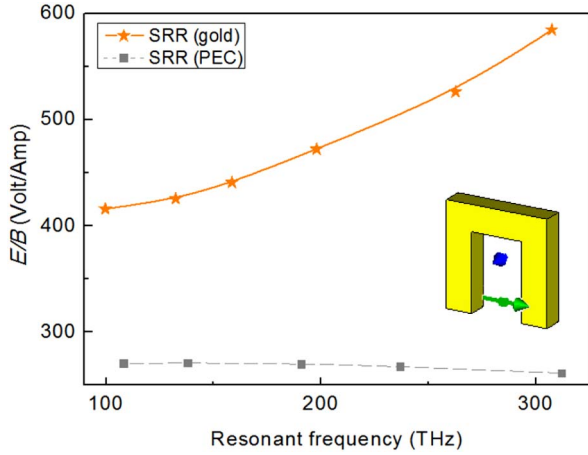


Fig. 4. Ratio of electric field (E) to magnetic field (B) of SRRs as a function of resonant frequencies. Inset shows that the electric field and the magnetic field are probed at the gap and the center of the SRR, respectively. The E/B ratio for an SRR made of PEC (gray dashed line) and gold (orange solid line) are shown for comparison.

$$\begin{aligned}
 U = & U_0 - \frac{1}{2} \epsilon_0 \epsilon_{ij} E_i E_j - \frac{1}{2} \mu_0 \mu_{ij} H_i H_j \\
 & - \frac{1}{3} \epsilon_0 \chi_{ijk}^{(2)} E_i E_j E_k - \frac{1}{3} \epsilon_0 \mu_0 \eta_{ijk}^{(2)} E_i E_j H_k - \frac{1}{3} \epsilon_0 \mu_0 \zeta_{ijk}^{(2)} E_i H_j H_k \\
 & - \frac{1}{4} \epsilon_0 \chi_{ijkl}^{(3)} E_i E_j E_k E_l + \dots, \quad (3)
 \end{aligned}$$

where the terms of the second line represent the Pockels effect, the Faraday effect (or magneto-optical Kerr effect), and the Cotton–Mouton effect, respectively. The term of the third line represents the Kerr effect.

The results discussed in previous sections indicate the capabilities of localized surface plasmons for probing the environmental magnetic media decrease at high frequencies. Physically, it indicates disparities of electric and magnetic field enhancements at high frequencies. As shown in Fig. 4, we use an SRR as an example and numerically calculate the ratio of electric to magnetic field-enhancements (E/B) for different resonant frequencies. As expected, an SRR made of PEC always displays its E/B being independent of resonant frequencies. On the other hand, when the SRR is made of gold ($\omega_{p,\text{Au}} = 2.175 \times 10^{15}$ Hz), the presence of localized surface plasmons leads to stronger electric field enhancements over those of a magnetic field, which manifests at the increased E/B at high resonant frequencies, as shown in Fig. 4. Thus, for a given incident electromagnetic wave, the Pockels effect or the Kerr effect will be greatly amplified by the electric field enhancements at the electromagnetic hot spots. On the other hand, the Faraday effect, the magneto-optical Kerr effect,

and the Cotton–Mouton effect can be enhanced as well, though are less pronounced.

From Eq. (3), the polarization (P) and the magnetization (M) can be obtained via $P = -\partial U / \partial E$ and $M = -\partial U / \partial H$, respectively. Experimentally, although the nonlinear coefficients of the Faraday effect and the Cotton–Mouton effect are always experimentally determined from the nonlinear refractive index, and their contributions to magnetizations are not usually mentioned in nonlinear optics, we note that the two effects can always contribute to nonlinear magnetizations. The nonlinear magnetization, as well as the nonlinear polarization, can be probed by the localized surface plasmons via scattered light or resonant frequency changes. However, due to the reduced sensitivity to μ , the nonlinear magnetizations induced by the Faraday effect or the Cotton–Mouton effect become difficult to be probed by localized surface plasmons at optical frequencies. Particularly, because the μ sensitivities become much reduced at high frequencies, the nonlinear signals will be much weaker for sum frequency generation than those for difference frequency generation. Likewise, rough surfaces of the plasmonic metal structures will play equivalent roles similar to the mixed real/spoof plasmons, leading to redshifting the resonant frequencies and reducing the nonlinear magnetic responses as shown in Fig. 2(d). Therefore our results put a fundamental constraint for all plasmon-assisted nonlinear magnetic phenomena.

This work was supported by the National Science Council of Taiwan (NSC101-2112-M-002-014-MY3) and National Taiwan University (NTU-CDP-102R7852).

References

1. P. W. Anderson, *Phys. Rev.* **130**, 439 (1963).
2. Y. K. Chang, Z. X. Lou, K. D. Chang, and C. W. Chang, *Opt. Express* **21**, 1804 (2013).
3. V. I. Belotelov, I. A. Akimov, M. Pohl, V. A. Kotov, S. Kature, A. S. Vengurlekar, A. V. Gopal, D. R. Yakovlev, A. K. Zvezdin, and M. Bayer, *Nat. Nanotechnol.* **6**, 370 (2011).
4. V. V. Temnov, *Nat. Photonics* **6**, 728 (2012).
5. J. Y. Chin, T. Steinle, T. Wehler, D. Dregely, T. Weiss, V. I. Belotelov, B. Stritzker, and H. Giessen, *Nat. Commun.* **4**, 1599 (2013).
6. M. M. Miller and A. A. Lazarides, *J. Phys. Chem. B* **109**, 21556 (2005).
7. C. Y. Chen, S. C. Wu, and T. J. Yen, *Appl. Phys. Lett.* **93**, 034110 (2008).
8. J. Zhou, T. Koschny, M. Kafesaki, E. N. Economou, J. B. Pendry, and C. M. Soukoulis, *Phys. Rev. Lett.* **95**, 223902 (2005).
9. J. B. Pendry, L. Martin-Moreno, and F. J. Garcia-Vidal, *Science* **305**, 847 (2004).
10. A. Pors, E. Moreno, L. Martin-Moreno, J. B. Pendry, and F. J. Garcia-Vidal, *Phys. Rev. Lett.* **108**, 223905 (2012).